Geochemistry, Geophysics, Geosystems®

RESEARCH ARTICLE
10.1029/2025GC012457

# What Controls Finger-Shaped Transformation Patterns? A Numerical Approach to Eclogitization

**A. Cochet[1], P. Yamato[1], M. Baïsset[1,2], T. Duretz[3], and L. Labrousse[4]**

[1]Univ Rennes, CNRS, Géosciences Rennes - UMR 6118, Rennes, France, [2]Université PSL, CNRS, Laboratoire de Géologie de l'ENS, UMR8538, Paris, France, [3]Institüt für Geowissenschaften, Goethe Universität, Frankfurt am Main, Germany, [4]Sorbonne Université, CNRS-INSU, Institut Des Sciences de La Terre Paris, ISTeP, UMR7193, Paris, France

**Abstract** Metamorphic transformations in subduction lithosphere are triggered by pressure and temperature changes occurring under stress. This anisotropic stress field can in turn be locally altered by the transformation pattern, as reactions induce significant changes of the material properties of the rocks. The granulite to eclogite transformation constitutes a striking example of a pressure-driven transformation potentially able to generate significant volume forces due to densification and known to be associated with transient weakening. However, the feedback mechanisms between pressure variations and the evolution of the physical properties of rocks during eclogitization remain poorly constrained. Formalizing these interactions is thus required to understand how eclogitization initiates and propagates under stress. In this study, mechanical numerical models are used to explore the evolution of eclogitization in a matrix-inclusion system subjected to shear boundary conditions, where pressure variations control the physical properties of the materials. Our results show that the initiation of the transformation is controlled by both the strength of the protolith and by the degree of overstepping of the transformation. Eclogite structures then systematically propagate in the direction normal to the principal shortening direction. In contrast, other parameters such as the density variations involved in the transformation, the initial difference in strength between the protolith and the inclusion, and the shape and orientation of the inclusion do not play a major role on the transformation initiation itself but enhance or inhibit its propagation.

**Plain Language Summary** When rocks undergo changes in pressure and temperature, such as in tectonic collision zones, their physical properties can be drastically altered by mineral transformations. For instance, the eclogite transformation of the lower crust, a pressure-driven transformation, generates a significant densification of the rocks that can in turn modify the surrounding pressure field. However, the feedback mechanisms that control how pressure and density variations interact to promote or inhibit the initiation and the propagation of this transformation through the rock remain poorly understood. To investigate this, we use numerical models where the physical laws that govern the evolution of material properties with pressure and temperature through a densification transformation have been implemented. These models involve the deformation of an elliptical inclusion placed within a surrounding material (matrix) that has different physical properties. Our results show that the pressure at which the transformation begins, as well as the ability of the original rock to deform under stress (strength) play a significant role in the initiation of the transformation. In contrast, other parameters like the change in density during the transformation and the difference in strength between the inclusion and the surrounding material, affect the enhancement or inhibition of its propagation.

**Key Points:**

- We use a 2-D numerical model to study the propagation of a pressure-driven transformation in a rock with an initial mechanical heterogeneity
- Initiation of the eclogite transformation is driven by local pressure variations generated by the mechanical heterogeneity of the rock
- Eclogitization, enhanced by viscosity contrasts and limited by densification, propagates normal to the principal shortening direction

**Supporting Information:**

Supporting Information may be found in the online version of this article.

**Correspondence to:**

A. Cochet and P. Yamato,
anais.cochet@univ-rennes.fr;
philippe.yamato@univ-rennes.fr

**Citation:**

Cochet, A., Yamato, P., Baïsset, M., Duretz, T., & Labrousse, L. (2025). What controls finger-shaped transformation patterns? A numerical approach to eclogitization. *Geochemistry, Geophysics, Geosystems*, *26*, e2025GC012457. https://doi.org/10.1029/2025GC012457

Received 20 MAY 2025
Accepted 19 OCT 2025

**Author Contributions:**

**Conceptualization:** A. Cochet, P. Yamato, L. Labrousse
**Data curation:** A. Cochet
**Funding acquisition:** P. Yamato
**Investigation:** A. Cochet
**Methodology:** A. Cochet, P. Yamato, T. Duretz
**Project administration:** P. Yamato
**Software:** P. Yamato, T. Duretz
**Supervision:** P. Yamato, M. Baïsset, T. Duretz, L. Labrousse



## 1. Introduction

When buried at depth in convergent zones, the lower continental crust is subjected to pressure ($P$) and temperature ($T$) changes (England & Thompson, 1984). These variations in $P$-$T$ conditions generate a thermodynamic disequilibrium within the rocks, that constitutes a driving force for metamorphic reactions. These mineralogical transformations can have a significant impact on both long-term lithosphere dynamics (Heténi et al., 2021; Jackson et al., 2004; Jung & Green, 2004; Kirby et al., 1996) and short-term processes (Austrheim & Boundy, 1994; Hacker et al., 2003; Lund & Austrheim, 2003; Lund et al., 2004; Shi et al., 2018) as they are associated with variations of the physical properties of the rocks, in particular changes in density and strength. While the significance of transformational weakening either due to the nucleation of intrinsically weak reaction products (e.g., Holyoke III & Tullis, 2006) or through the activation of grain-size sensitive deformation processes in transformed areas (e.g., Brodie & Rutter, 1987) has been widely studied, it appears more difficult to conclusively demonstrate the effects of a change in density. Recent studies based on thermo-mechanical models

**Validation:** A. Cochet, P. Yamato, M. Baïsset, L. Labrousse
**Visualization:** A. Cochet
**Writing – original draft:** A. Cochet
**Writing – review & editing:** A. Cochet, P. Yamato, M. Baïsset, T. Duretz, L. Labrousse

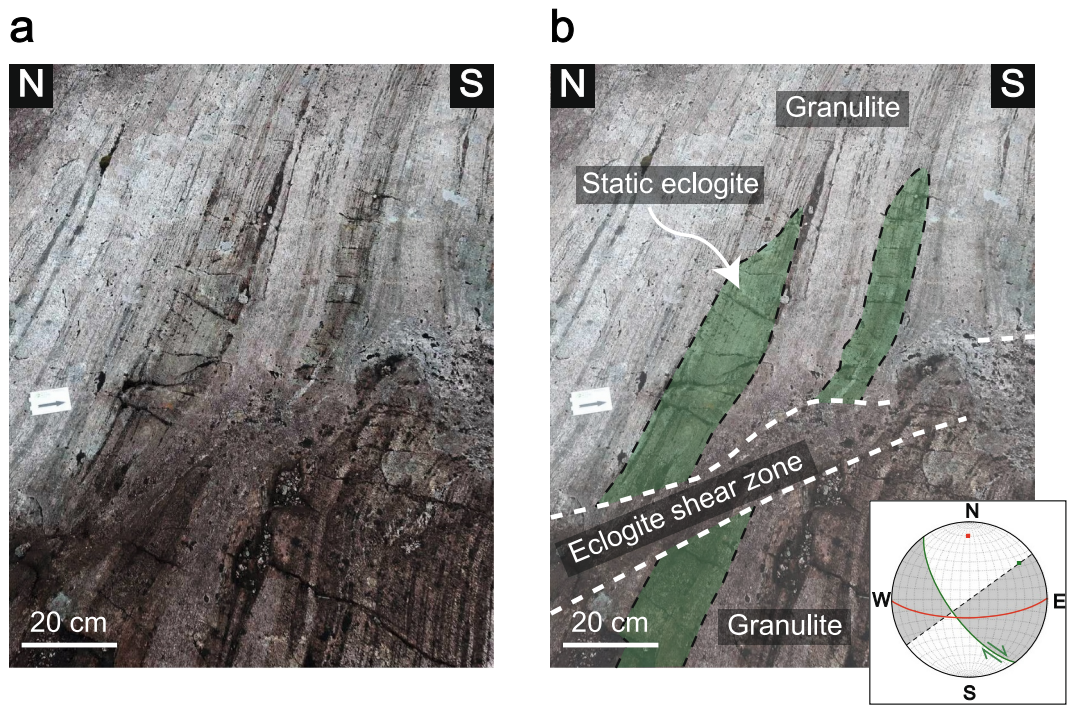


**Figure 1.** Photograph of partially eclogitized granulites from Holsnøy (a) and its interpretation (b) (60°N35'35, 005°E01'47). Eclogite finger (light green in b) rooted on an eclogite shear zone (between the white dashed lines in b). Stereographic plot in b: shear zone in green (shear plane, shear direction and pole to shear plane) and eclogite finger in red (finger plane and pole to this plane). Dilatation quadrants (in white) and compression quadrants (shaded) are defined by the shear plane and by the vertical plane that contains the pole to shear plane.

or field data have shown that density variations can strongly affect the propagation pattern of pressure-driven transformations, suggesting that they either impact the local stress field (Baïsset et al., 2023, 2025; Putnis et al., 2021) or enhance the creation of porosity which modifies the permeability and fluid flow (Bras et al., 2023; Jamtveit et al., 2000; Schmalholz et al., 2023, 2024; Yamato et al., 2022; Zertani, Labrousse, et al., 2019). While density and viscosity variations can be studied independently in numerical models, the effects of these physical properties are intrinsically entangled in naturally deformed rocks. The world-famous island of Holsnøy in the Scandinavian Caledonides of Norway, constitutes a perfect field example to study such a link between eclogite-facies transformations and the rheology of reacting rocks (Austrheim, 1987; Putnis et al., 2017). Careful analysis of eclogite-facies zones in this massif initially composed of continental granulites indeed reveals a complex interplay between deformation and reactions. Two types of eclogite-facies structures can be identified: (a) eclogite shear zones and (b) finger-shaped eclogite fronts (the so-called 'eclogite fingers') that propagate into the granulites without macroscopic deformation (Austrheim, 1987; Baïsset, 2023; Baïsset et al., 2025; Putnis et al., 2021; Zertani, Labrousse, et al., 2019) (Figure 1). The presence of both deformed and undeformed reaction zones is puzzling, prompting several key questions: how to initiate such finger-shaped eclogite structures? How do they spatially propagate under a regional stress field? Why do eclogite fingers stop and how are they preserved as 'static' structures inside the reacting granulites?

Four main studies have proposed a mechanism for finger propagation. It has first been proposed that when dry anorthosite transforms into eclogite, the associated densification induces fracturing at the fingertip. This fracturing facilitates fluid infiltration, which in turn enhances reaction and leads to a self-sustaining feedback process. According to this model, the development of eclogite fingers requires an anisotropy of the stress field, such that the rock is closer to the brittle yield criterion in some directions than in others (Jamtveit et al., 2000). Some other studies instead showed that fingers preferentially develop along the granulite foliation (Baïsset et al., 2025; Putnis et al., 2021; Zertani et al., 2022). In particular, it has been proposed that the fingertip corresponds to the location where fluids have migrated the farthest from their source in the shear zone. In addition, they emphasize that granulite remains hydrated beyond the fingertip, and propose that pressure rather than fluid availability is the

main controlling factor for the shape and propagation of the fingers (Putnis et al., 2021). Another study argues that once the reaction has been initiated, the porosity generated by the volume change becomes the main driver of fluid transport and, consequently, of finger propagation (Zertani et al., 2022). Based on field observations, Baïsset et al. (2025) report a non-random distribution of fingers. They conclude that the stress field must be favorably oriented relative to the granulite foliation for efficient finger propagation. In their conceptual model fluids also play a significant role as they are likely to migrate more easily along the foliation than across, their flow being controlled by both pressure and porosity gradients. In summary, two main hypotheses have been proposed to explain finger-shaped eclogite propagation:

1. The eclogitization of initially dry granulites is responsible for a significant densification of the rocks that is accommodated by the opening of pores. A runaway process then occurs: fluids flow in the rock that became more porous and permeable due to the reaction and then enhance the eclogite transformation which in turn increases the permeability of the rock (Bras et al., 2023; Jamtveit et al., 2000; Schmalholz et al., 2024; Yamato et al., 2022; Zertani et al., 2022). This process stops when all the fluids are consumed.
2. The initial background pressure is lower than the pressure of the transformation. The rock contains a limited volume of free fluids at grain boundaries. This volume is sufficient to kinetically allow equilibration of the granulitic paragenesis (feldspar, pyroxene and garnet) into higher pressure minerals (e.g., Na-rich pyroxene and Ca-rich garnet) at eclogite facies conditions, but small enough such that the pressure required for this transformation has not been reached. Local pressure variations generated by the mechanical heterogeneities of the rock are responsible for the initiation of the eclogitization transformation (Putnis et al., 2021). In this case, pressure drives the eclogitization process and when it decreases below the background pressure, eclogitization stops.

Both scenarios imply pressure variations. In the first case, fluid pressure gradients are required to enhance fluid propagation within an initially anhydrous rock through the formation of cracks and porosity. In the second case, a mechanism is necessary to generate enough local pressure and reach the pressure of transformation. Field data show that transformation from granulite to eclogite is associated with densification and softening, two processes that are intrinsically linked to pressure variations. While the specific effects of density and viscosity variations have not been examined in detail, few recent studies suggest that reaction softening is necessary for the propagation of finger-like fronts, in the case where transformation induces density variations (Schmalholz et al., 2023; Yamato et al., 2022). The aim of this study is therefore to investigate the impact of these parameters and to identify the conditions favorable to eclogitization (for a given temperature and chemical composition), as well as to understand the propagation of the transformation front and the formation of fingers.

In the following, we present the results of a parametric study on the deformation of a single phase visco-elasto-plastic material using compressible two-dimensional (2D) mechanical numerical models. Different parameters are tested: (a) the pressure difference between the pressure of the transformation and the initial background pressure ($\Delta P$), (b) density variations caused by the transformation ($\Delta\rho$) (c) viscosity ratios between the initial material and the product of the transformation as well as (d) the shape and size of the inclusion. The results obtained are then discussed in the light of previous numerical studies, and are also compared to field observations, with the aim of shedding light on the conditions that favor or hinder finger-shaped eclogite propagation.

## 2. Methods

### 2.1. Model Design

We simulate the propagation of the eclogitization transformation in a granulite matrix (Figure 2). A weak inclusion is placed in the center of the model and a constant strain rate is applied as boundary conditions ($\dot{\epsilon}_{BG} = 10^{-14}\ s^{-1}$; Figure 2a). The weak inclusion may represent shear zones in the early stages of their development if we consider the mineral assemblage at the onset of the reactions (Bras et al., 2021). The entire study is presented here under pure shear conditions. The test performed with the reference model under simple shear indicates that the results are also valid in this configuration (see Figure S1 in Supporting Information S1). The temperature remains constant during the whole simulation ($T_{BG} = 680°C$) and the background pressure ($P_{BG}$) is considered lower than the pressure of the transformation ($P_t$). We define a reference model in which a pressure increase of 200 MPa is required to trigger the transformation (i.e., $P_t = 1.8$ GPa and $P_{BG} = 1.6$ GPa, see Figure 2b). In areas where the pressure reaches the transformation pressure, the viscosity and density of the material are modified (Figure 2c).

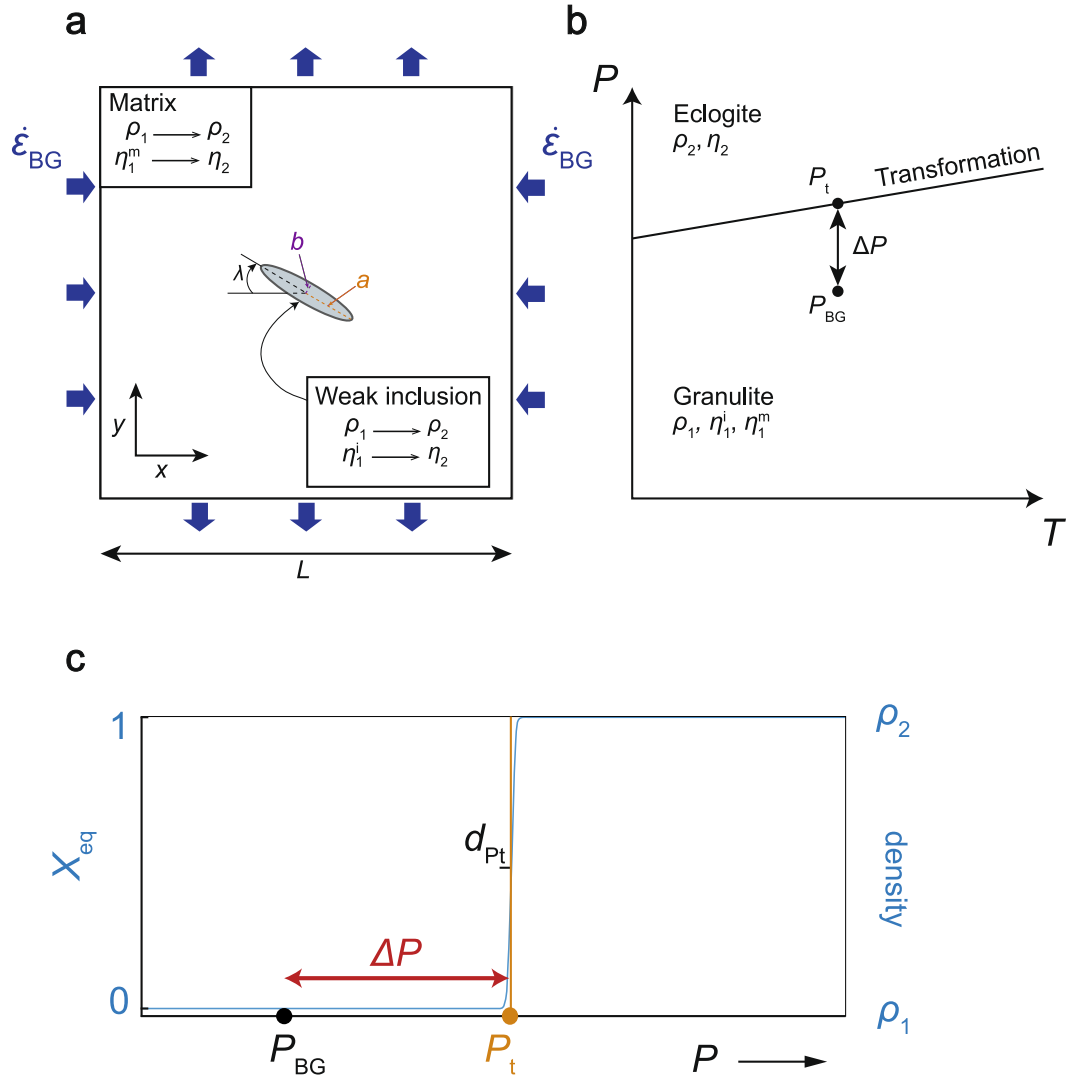


**Figure 2.** Initial configuration. (a) Model setup: a background strain rate $(\dot{\varepsilon}_{BG})$ is applied as pure shear boundary conditions (dark blue arrows). The elliptic inclusion at the center of the model has a lower viscosity $(\eta_1^i)$ than the matrix ($\eta_1^m$, see Table 2). (b) Pressure ($P$) - temperature ($T$) diagram presenting the position of a pressure-controlled transformation (black line) associated with density and viscosity variations (from $\rho_1$ to $\rho_2$ and from $\eta_1^i$ or $\eta_1^m$ to $\eta_2$, respectively). (c) Evolution of the transformation progress ($X_{eq}$) as a function of pressure. $\Delta P$ corresponds to the difference between the background pressure $(P_{BG})$ and the pressure of the transformation $(P_t)$ at a given temperature. $d_{Pt}$ is the pressure standard deviation that controls the evolution of the transformation extent with pressure for a given value of $P_t$.

### 2.2. Description of the Numerical Code

#### 2.2.1. Mechanical Equations

In this study, we use the 2-D mechanical code MDoodz7.0 that allows to account for the visco-elasto-viscoplastic (V-E-VP) rheology of rocks (Duretz et al., 2019, 2021; Yamato et al., 2019). The code solves a set of partial differential equations that are discretized using a staggered finite difference scheme and markers-in-cell method (at least 16 markers per cell) (Gerya, 2019; Yamato et al., 2019). The spatial components of the velocities $V_x$ and $V_z$ and the pressure $P$ are obtained by implicitly solving the Eulerian equations of momentum and continuity (Stokes equations), which are expressed as:

$$-\frac{\mathrm{d}\ln(\rho)}{\mathrm{d}t} = \frac{\partial V_i}{\partial x_i} \quad (1)$$

**Table 1**
*General Parameters of the Models*

| Symbol | Meaning | Unit | Value |
|---|---|---|---|
| $P_{BG}$ | Initial pressure | GPa | 1.6 |
| $P_t$ | Pressure of the transformation | GPa | 1.8 |
| $d_{Pt}$ | $P_t$ standard deviation | MPa | 50 |
| $\dot{\varepsilon}_{BG}$ | Background strain rate | $s^{-1}$ | $1 \times 10^{-14}$ |
| $T_{BG}$ | Background temperature | °C | 680 |
| $C_p$ | Heat capacity | $J.kg^{-1}.K^{-1}$ | 1,050 |
| $k$ | Conductivity | $W.m^{-1}.K^{-1}$ | 2.3 |
| $K$ | Bulk modulus | GPa | 80 |
| $G$ | Shear modulus | GPa | 40 |
| C | Cohesion | MPa | 50 |
| $\varphi$ | Friction angle | ° | 30 |
| $\eta_{VP}$ | Viscoplastic viscosity | Pa.s | $5 \times 10^{19}$ |
| $t_k$ | Characteristic time for the transformation | s | $3.1558 \times 10^{10}$ |
| $k_{chem}$ | Chemical diffusion coefficient | $m^2.s^{-1}$ | $1 \times 10^{-15}$ |
| $L$ | Model height at initial state | m | 2 |
| $a$ | Length of the semi-major axis of the ellipse | m | 0.1 |
| $b$ | Length of the semi-minor axis of the ellipse | m | 0.1 |
| $\lambda$ | Angle between the major axis of the ellipse and the shortening direction $\sigma_1$ | ° | - |

$$\frac{\partial \sigma_{ij}}{\partial x_j} = 0 \tag{2}$$

in the case of a compressible material, neglecting both gravity and inertial terms. $\rho$ is the density and $V_i$ the velocity in direction $i$. $\sigma_{ij}$ is the stress tensor and $x_i$ the spatial coordinate in direction $i$.

### 2.2.2. Rheological Model

In our models, materials can deform elastically, viscously and frictionally depending on the $P$-$T$ conditions and the applied strain rate. The total strain rate is expressed as:

$$\dot{\varepsilon}_{ij} = \dot{\varepsilon}^{v}_{ij} + \dot{\varepsilon}^{e}_{ij} + \dot{\varepsilon}^{vp}_{ij} \tag{3}$$

where the exponents e, v, and vp correspond to the elastic, viscous and viscoplastic components of the strain rate, respectively. To calculate these three components, we need to consider the effective stresses associated with the different deformation modes. The elastic strain rate is defined by the Hooke's law as:

$$\dot{\varepsilon}^{e}_{ij} = \frac{D}{Dt}\left(\frac{\tau_{ij}}{2G}\right) \tag{4}$$

where $G$ is the shear modulus (see Table 1) and $\tau_{ij}$ is the deviatoric stress tensor. For viscous deformation, we only consider dislocation creep rheology. The flow stress $(\tau_f)$ is thus calculated as:

$$\tau_f = 2F_{pwl}A^{-\frac{1}{n}} \exp\left(\frac{Q}{nRT}\right)\dot{\varepsilon}^{v\frac{1}{n}}_{II} \tag{5}$$

**Table 2**
*Physical Parameters of the Materials in the Reference Model*

| Symbol | Meaning | Unit | Value |
|---|---|---|---|
| Matrix (dry anorthite) | | | |
| $A$ | Pre-exponential factor (dislocation creep)[a] | $Pa^{-n}.s^{-1}$ | $5.0119 \times 10^{-6}$ |
| $n$ | Stress exponent[a] | – | 3 |
| $Q$ | Activation energy (dislocation creep)[a] | $kJ.mol^{-1}$ | 648 |
| $\rho_1$ | Initial density (before transformation) | $kg.m^{-3}$ | 2,850 |
| Inclusion (wet anorthite) | | | |
| $A$ | Pre-exponential factor (dislocation creep)[b] | $Pa^{-n}.s^{-1}$ | $3.9811 \times 10^{-16}$ |
| $n$ | Stress exponent[b] | – | 3 |
| $Q$ | Activation energy (dislocation creep)[b] | $kJ.mol^{-1}$ | 356 |
| $\rho_1$ | Initial density (before transformation) | $kg.m^{-3}$ | 2,850 |
| Product of the transformation (omphacite) | | | |
| $A$ | Pre-exponential factor (dislocation creep)[c] | $Pa^{-n}.s^{-1}$ | $1 \times 10^{-23}$ |
| $n$ | Stress exponent[c] | – | 3.5 |
| $Q$ | Activation energy (dislocation creep)[c] | $kJ.mol^{-1}$ | 356 |
| $\rho_2$ | Final density (after transformation) | $kg.m^{-3}$ | 2,950 |

[a]From Rybacki and Dresen (2000) for dry anorthite. [b]From Rybacki and Dresen (2000); Rybacki and Dresen (2004) for wet anorthite. [c]From Zhang et al. (2006) for omphacite.

where $R$ is the universal gas constant ($R = 8.314510\ J.K^{-1}.mol^{-1}$) and $n, A, Q$ are the dislocation creep parameters of the material (see Table 2). $F_{pwl}$ is a correction factor for invariant formulation relative to the type of experiments used for calibration (here axial compression), expressed as follows (Schmalholz & Fletcher, 2011):

$$F_{pwl} = \frac{1}{6} 2^{\frac{1}{n}} 3^{\frac{n-1}{2n}} \tag{6}$$

It is then possible to define the viscous strain rate using Equation 5 such as:

$$\dot{\varepsilon}_{ij}^{v} = \dot{\varepsilon}_{II}^{v} \frac{\tau_{ij}}{\tau_{II}} = A \left[ 2F_{pwl} \exp\left(\frac{Q}{nRT}\right) \right]^{-n} \tau_f^n \frac{\tau_{ij}}{\tau_{II}} \tag{7}$$

where $\dot{\varepsilon}_{II}^{v}$ is the square root of the second invariant of the viscous strain rate tensor and $\tau_{II}$ is the second invariant of the deviatoric stress. To account for frictional behavior, we impose a yield stress ($\tau_y$) computed from the viscoplastic Drucker-Prager law as:

$$\tau_y = C\cos(\phi) + P\sin(\phi) + 2\eta^{vp}\dot{\varepsilon}_{II}^{vp} \tag{8}$$

where $C$ is the cohesion and $\phi$ the angle of friction of the material. To ensure the convergence of the solution with the resolution, a viscoplastic parameter ($\eta^{vp}$) is added to the yield stress equation (Duretz et al., 2020). This value has been chosen in order to limit the overstress to 1 MPa on average (i.e., $\eta^{vp} = 5 \times 10^5$ Pa.s for $\dot{\varepsilon}_{II}^{vp} = 10^{-14} s^{-1}$). Eventually, the plastic strain rate can be calculated using the total strain rate equation (Equation 3) as:

$$\dot{\varepsilon}_{ij}^{vp} = \dot{\varepsilon}_{II}^{vp} \frac{\tau_{ij}}{\tau_{II}} = \left[ \dot{\varepsilon}_{II} - \frac{\dot{\tau}_{II}}{2G} - \frac{\tau_{II}}{2\eta} \right] \frac{\tau_{ij}}{\tau_{II}} \tag{9}$$

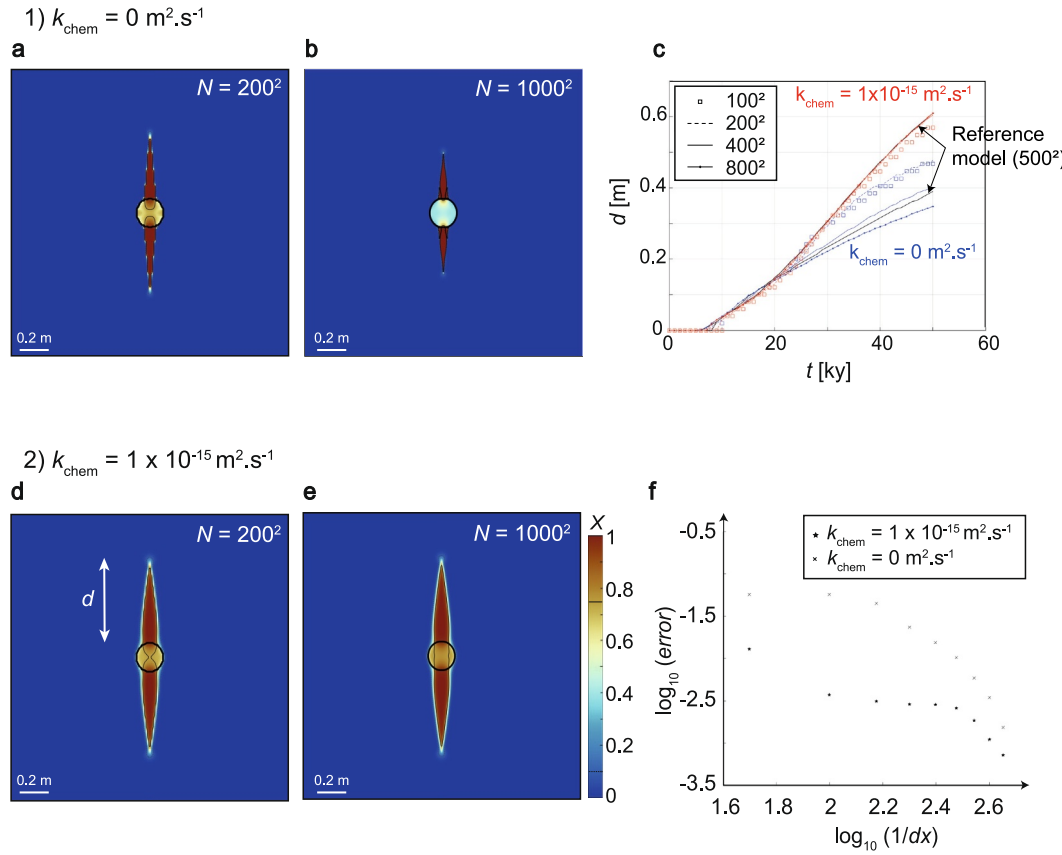


**Figure 3.** Convergence tests. Comparison of a model where $k_{chem} = 0$ m$^2$s$^{-1}$ (a, b) and a model where $k_{chem} = 1 \times 10^{-15}$ m$^2$s$^{-1}$ (d, e). (c) Length of the eclogite finger $d$ with time showing the convergence of the models. The reference model corresponds to a model with a resolution of 500 × 500 (black lines). (f) Difference between the highest resolution model (1000 × 1000) and models with lower resolution (see Equation 14).

### 2.2.3. Metamorphic Transformations

In our model, the pressure-driven metamorphic transformation occurs in places where the pressure $P$ exceeds the pressure of the transformation $P_t$. The transformation progress at equilibrium ($X_{eq}$) is a function of $P$ and follows a cumulative distribution function for a normal distribution (S-shape curve, Figure 2c) defined by the equation:

$$X_{eq} = 1 - \frac{1}{2}\left(\mathrm{erfc}\left(\frac{P - P_t}{d_{Pt}}\right)\right) \tag{10}$$

where $d_{Pt}$ is the pressure standard deviation added to smooth the function and avoid numerical issues (Yamato et al., 2022). The evolution of the amount of transformation $X$ over time is calculated by introducing a characteristic time for the transformation $t_k$ (in s) and a chemical diffusion coefficient $k_{chem}$ (in m$^2$.s$^{-1}$), such as:

$$\frac{dX}{dt} = \frac{X_{eq} - X}{t_k} + \frac{\partial}{\partial x_i}\left(k_{chem}\frac{\partial X}{\partial x_i}\right) \tag{11}$$

$t_k$ is a 'kinetics' term, $1/t_k$ corresponding to the transformation rate of the first order Avrami's law (e.g., Poirier, 1982). $k_{chem}$ controls the diffusion of $X$, a process that can simulate the diffusion of chemical elements during the transformation and therefore mimic the diffusion of the transformation front. This parameter greatly improves the convergence of the model with resolution (Figure 3). While the transformation progresses in the model, viscosity and density of the transforming material evolve toward those of the transformation product (Table 2).

These properties are calculated at each time step following the Minimized Power Geometric model for viscosity (Huet et al., 2014, see their Table 2), and expressed as follows for density:

$$\rho_0 = X\rho_1 + (1 - X)\rho_2 \tag{12}$$

where $\rho_0$ is the reference density, $\rho_1$ is the initial reference density and $\rho_2$ is the final reference density. The reference density $\rho_0$ is then used to calculate the effective density ($\rho$), which depends on the pressure according to:

$$\rho = \rho_0 \exp(\beta P) \tag{13}$$

where $\beta = 1/K$ is the compressibility with $K$ the bulk modulus of the material (see Table 1).

### 2.3. Choice of Physical Parameters

Parameters for the reference model were chosen to be as close as possible to the natural values reported in the literature for the granulite to eclogite transformation as observed in Holsnøy. They are presented in Tables 1 and 2. The matrix is considered as dry anorthite (flow law parameters from Rybacki & Dresen, 2000) while the elliptical inclusion is considered as wet anorthite (0.007 wt% $H_2O$; flow law parameters from Rybacki & Dresen, 2000; Rybacki & Dresen, 2004), a material that is two orders of magnitude weaker than the matrix at the considered conditions. A friction angle $\phi = 30°$ and a cohesion $C = 50$ MPa were considered for the frictional behavior (Equation 8) as in Byerlee's law (Byerlee, 1978). The temperature of the simulations ($T_{BG} = 680°C$) was chosen based on the estimates of Bhowany et al. (2017). The initial background pressure ($P_{BG}$) was set to 1.6 GPa in the reference model and then tested in the parametric study. As pressures recorded by the eclogites in Holsnøy lies between 1.6 and 2.0 GPa (Bhowany et al., 2017), we decided to set the pressure of the transformation ($P_t$) in between at 1.8 GPa. The density of the initial granulite is set to $\rho_1 = 2{,}850$ kg.m$^{-3}$ in the reference model. When the transformation is complete, the density of the transformed material is equal to that of eclogite: $\rho_2 = 2{,}950$ kg.m$^{-3}$ (i.e., a difference in density of 100 kg.m$^{-3}$ in comparison with the initial granulite). These values are of the same order of magnitude than those estimated by Austrheim (1987) for the densification induced by eclogitization of granulite-facies rocks in Holsnøy. In our study, the characteristic time $t_k$ for the transformation kinetics is set to 1,000 years. Such fast kinetics align with data from experimental petrology, combined with field observations from the partially eclogitized Holsnøy massif (Malvoisin et al., 2020). The background strain rate is set to $10^{-14}$ s$^{-1}$ (Fagereng & Biggs, 2019). The initial size of the model is 2 m × 2 m. The inclusion is located at the center of the model and initially elliptical in shape. Its ellipticity is controlled by the ratio between its longest axis ($a$) over its shortest axis ($b$). The angle between the longest axis and the maximum principal stress, $\sigma_1$, will be denoted as $\lambda$ throughout this study (Figure 2a).

In order to present and discuss the model results, we use the following metrics (a) the progress of the transformation $X$ that evolves from 0 (i.e., untransformed material) to 1 (i.e., fully transformed material) and (b) the dynamic pressure that corresponds to the difference between the (total) pressure $P$ and the initially imposed (lithostatic) background pressure $P_{BG}$. In addition, to quantify the spatial evolution of the eclogitic transformation, we also extract the length of the eclogite finger $d$ at each time step. This length is calculated as the distance between the edge of the inclusion and the maximum in $y$-coordinate where $X > 0.1$ (see Figure 3).

### 2.4. Verification and Robustness

In order to verify the model implementation, we first performed a simple simulation where a weak inclusion is deformed under pure shear and compare the results with the analytical solution proposed by Moulas et al. (2014). In order to fit the analytical solution, the initial reference conditions were simplified by considering both matrix and inclusion as non-reactive purely viscous materials with linear viscosities. We also imposed the ratio between the viscosity of the inclusion and the matrix $\eta^i/\eta^m = 0.1$ and the ellipticity $b/a = 3$ (Figure S2 in Supporting Information S1). In a second step, to test the implementation of our rheological laws, we performed pure shear deformation simulations of single-phase materials (either anorthite or omphacite) and compared the loading curves extracted from these simulations with the semi-analytical solutions that exists for this problem as done in Yamato et al. (2019). Results of these simulations perfectly fit the semi-analytical solutions. Also, we performed a model where the transformation is activated but only generates a density change. Results of this simulation are the

same as those of Yamato et al. (2022). For a potential variation of viscosity caused by the transformation, no analytical solution has ever been proposed in the literature. However, to ensure the robustness of our results, we tested the convergence of our models by calculating the error associated with the resolution of the model:

$$\text{error} = \frac{\sum \|d_{\text{ri}} - d_{\text{r1000i}}\|}{N} \tag{14}$$

where $d_{\text{ri}}$ corresponds to the finger length at a given time step and a given resolution. $d_{\text{r1000i}}$ is the finger length at the same time step for a model with a resolution of 1000 × 1000 cells, and $N$ is the number of time steps considered. The solution converges when the resolution increases in a log-log diagram of the calculated error as function of the inverse of the spatial discretization (Figure 3). In order to combine reasonable computation times with suitable resolution, all models were run with a spatial resolution of 500 × 500 cells.

### 2.5. Characteristic Parameters and Dimensionless Numbers

In our reference simulation, we specifically consider the eclogite transformation, represented by both viscosity and density variations, with material parameters constrained by natural data from Holsnøy, Norway. Results of this simulation are therefore presented in their dimensional form, with physical units. In contrast, results of the systematic studies are described using dimensionless numbers to make them applicable at different scales. Dimensionless numbers involve characteristic numbers, which are in our study the length ($L_c$), time ($t_c$), density ($\rho_c$), and viscosity ($\eta_c$). The characteristic length is defined by the initial length of the model ($L_c = 2$ m), while the characteristic time is calculated based on the background strain rate, following the relation $t_c = 1/\dot{\varepsilon}_{BG}$. Density has been normalized with respect to the initial density of the matrix ($\rho_c = \rho_1 = 2850$ kg.m$^{-3}$), and the characteristic viscosity is defined as the matrix viscosity at the beginning of the model ($\eta_c = \eta_1^m$). Finally, the pressure is normalized with respect to the background stress, calculated using the relation $\tau_c = 2 \times \eta_c \times \dot{\varepsilon}_{\text{BG}}$. All characteristic parameter values are provided in Table S1 in Supporting Information S1.

## 3. Results

### 3.1. Results From the Reference Model

Propagation of the transformation in the reference model takes place in the areas where the pressure is greater than the pressure of transformation $P_t$, that is, in the overpressure halos around the weak inclusion (Figure 4). At the beginning of the simulation (at $t = 0$ kyr), the transformation did not start (Figure 4a) because the pressure in the model has not yet reached the transformation pressure $P_t = 1.8$ GPa. When $P > P_t$, transformation starts and propagates perpendicularly to the shortening direction, forming a finger-like structure. The first areas that transform are at the outer edges of the inclusion, perpendicular to the shortening direction, but the inclusion itself does not react at this stage, because the dynamic pressure is zero inside a circular inclusion (Schmid & Podladchikov, 2003; Moulas et al., 2014, Figures 4b–4e). While transformation propagates, overpressures are also generated in the inclusion which eventually transforms (Figures 4c–4f). Transformation propagates in a self-sustained manner because the transformation product is weaker than the matrix and therefore generates additional overpressure at the tip of the transformed area (Figures 4e and 4f). Once the transformation starts, our results show that the propagation rate of eclogitization remains almost constant (Figure 4d). At the pressure, temperature and strain rate conditions imposed in this model, frictional deformation only occurs in the low-pressure areas close to the inclusion and does not affect the eclogite propagation (Figure S3 in Supporting Information S1).

### 3.2. Effect of Pressure, Density and Viscosity

This section presents the results of a parametric study performed on the relevant physical parameters for the considered transformation. These parameters are: (a) the difference in pressure between the pressure of the transformation and the initial pressure of the model: $\Delta P = P_t - P_{\text{BG}}$, (b) the difference between the final density of the reaction product (when $X = 1$) and the initial density of the transforming material (when $X = 0$): $\Delta\rho = \rho_2 - \rho_1$, and (c) the viscosity ratio between the reactant and the transformation product. The ranges of parameter values tested are provided in Table S2 in Supporting Information S1.

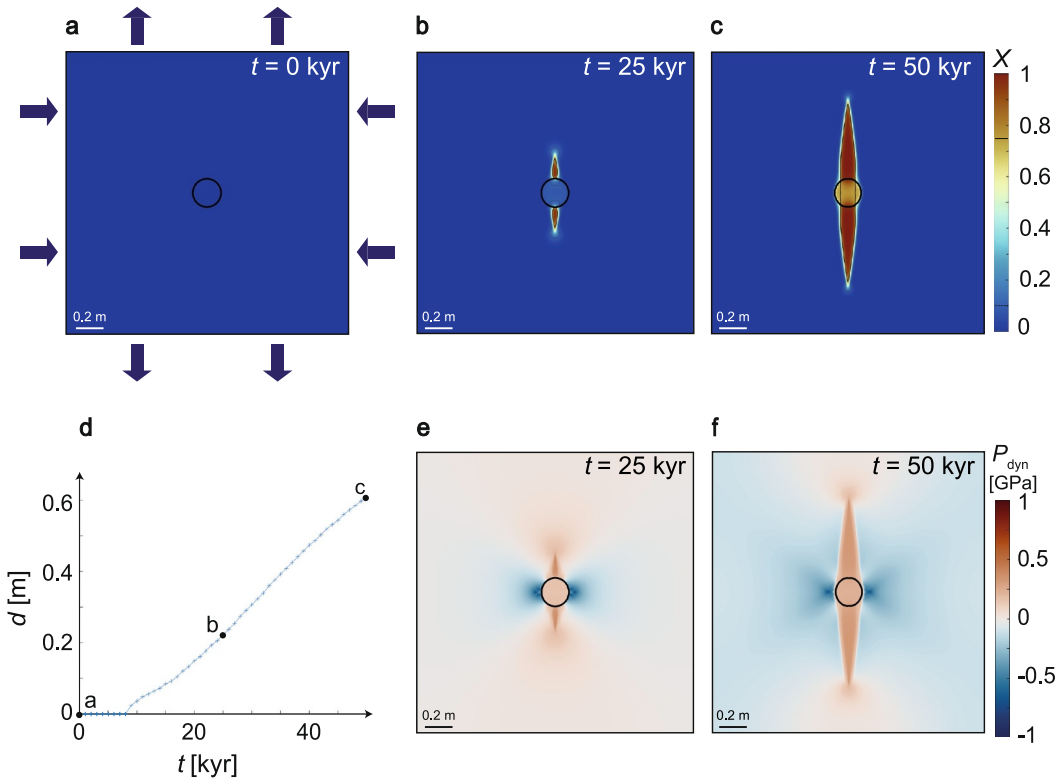


**Figure 4.** Evolution of eclogite propagation with time for the reference model. The transformation progress $X$ is shown at the initial stage (a), at 25 kyr (b) and at 50 kyr (c). The direction of principal stresses is represented by the dark blue arrows in (a). (d) Evolution of the length of the eclogite finger ($d$) with time. (e, f) Evolution of the dynamic pressure ($P_{dyn}$) with time.

### 3.2.1. Effect of the Difference Between the Pressure of the Transformation and the Background Pressure

Sixteen simulations were run with different values of the background pressure $P_{BG}$ for a given pressure of transformation $P_t$ to identify the impact of $\Delta P$ on the length of the eclogite finger (Figure 5). Results of these simulations show a non-linear decrease of the $d/L_c$ ratio when $\Delta P$ increases, up to a threshold value of $\Delta P/\tau_c = 1.15$ above which the transformation no longer takes place (Figure 5a). The decrease in $d/L_c$ observed with increasing $\Delta P$ suggests a reduction in the average propagation rate with $\Delta P$ (Figure S4 in Supporting Information S1). When $\Delta P/\tau_c$ is lower than 0.29, the measurements are limited by a boundary effect because the eclogite finger exceeds the height of the model box (Figure 5a). When $\Delta P$ is zero or negative, the metamorphic transformation propagates in a finger-like shape (Figures 5d and 5e). When $\Delta P$ is zero, the propagation rate is high enough for the finger length to exceed the model boundaries (Figure 5d). When $\Delta P$ is negative, the matrix undergoes slight transformation at an early stage, and an eclogite finger develops, propagating perpendicular to the shortening direction (Figure 5e and Figure S5 in Supporting Information S1). During the simulation, the matrix pressure decreases, causing the matrix to return to its initial state ($X = 0$, see Figure S5 in Supporting Information S1).

### 3.2.2. Effect of Transformation-Induced Density Variations

Fifteen values of the difference in density ($\Delta\rho$) between the untransformed material (i.e., initial matrix and inclusion) and the fully transformed material were tested (Figures 6a–6c). Results of these simulations show that a positive change in density (i.e., a densification) leads to a decrease of the finger length (Figure 6a). More specifically, a non-linear decrease of the finger length is observed when $\Delta\rho$ increases. After $t/t_c = 0.016$, $d/L_c$ is lower than 0.1 for $\Delta\rho/\rho_c = 0.11$ (Figures 6a and 6c). The transformation propagates more efficiently when $\Delta\rho/\rho_c = 0$ than when $\Delta\rho/\rho_c = 0.14$. Similarly to what was previously observed when $\Delta P/\tau_c < 0.29$ GPa (Section 3.2.1), the finger exceeds the height of the box for negative values of $\Delta\rho/\rho_c$ (Figures 6a and 6b). When negative values of $\Delta\rho$ are applied, the propagation initially develops perpendicular to the principal shortening

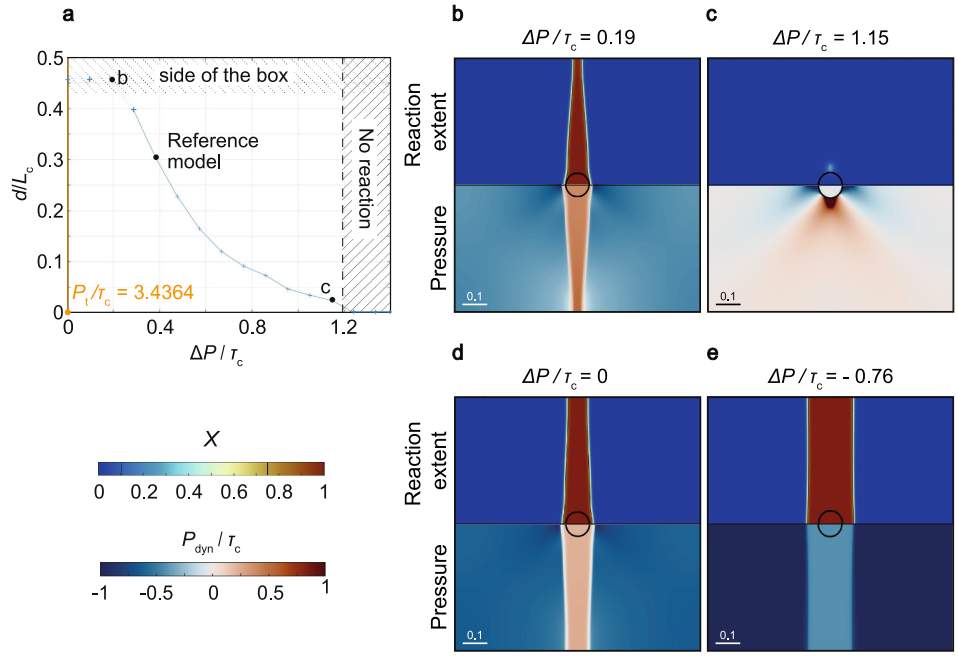


**Figure 5.** Effect of the difference in pressure between the pressure of the transformation and the background pressure ($\Delta P$). (a) Length of the eclogite finger as a function of $\Delta P$. (b,c,d,e) Reaction extent (top) and dynamic pressure field (bottom) for $\Delta P/\tau_c = 0.19$, $\Delta P/\tau_c = 1.15$, $\Delta P/\tau_c = 0$ and $\Delta P/\tau_c = -0.76$, respectively (after $t/t_c = 0.016$).

direction while widening laterally. For $\Delta\rho/\rho_c = -0.035$, the eclogite transformation is complete after $t/t_c = 0.0079$ (Figure 6d).

### 3.2.3. Effect of Transformation-Induced Viscosity Variations

Fifty-four models were run to investigate (a) the minimum value of the matrix viscosity ($\eta^m$) and (b) the minimum value of the viscosity ratio between the matrix and the inclusion $(\eta^m/\eta^i)$ required to trigger the transformation (Figure 7a). These runs were performed using linear viscosities, without plasticity and using the same value for the viscosity of the final product as the initial viscosity of the inclusion. Results of these simulations show that the transformation does not propagate when $\log_{10}(\eta^m/\eta_c)$ is less than or equal to −0.8, whatever the value of $\eta^m/\eta^i$ is (Figure 7a). Above this value, the length of the eclogite finger increases with increasing values of $\eta^m$. The length of the eclogite finger also increases with increasing values of $\eta^m/\eta^i$. Obviously, when there is no viscosity contrast between the matrix and the inclusion (i.e. $\eta^m/\eta^i = 1$), the transformation does not occur.

In a second step, 36 simulations were run with $\eta^m/\eta_c$ set at 0.38 for different values of the initial viscosity of the inclusion $(\eta^i)$ and of the final viscosity of the transformation product $(\eta_2)$ (Figure 7b). Results show that the value of $\eta^m/\eta_2$ has no influence on the onset of the transformation and has a limited impact on the final length of the finger.

Eventually, we performed a last series of models with stress-dependent (non-linear) viscosities (see Equation 5). For this, we define the viscosity as:

$$\eta = \eta_0 \cdot \dot{\varepsilon}^{\frac{1}{n}-1} \tag{15}$$

and ensure that this viscosity is equal to $\eta_{ref} = 10^{23}$ Pa.s when $\dot{\varepsilon}_{ref} = 10^{-14}$ s$^{-1}$ by computing $\eta_0$ as:

$$\eta_0 = \frac{\eta_{ref}}{\dot{\varepsilon}_{ref}^{\frac{1}{n}-1}} \tag{16}$$

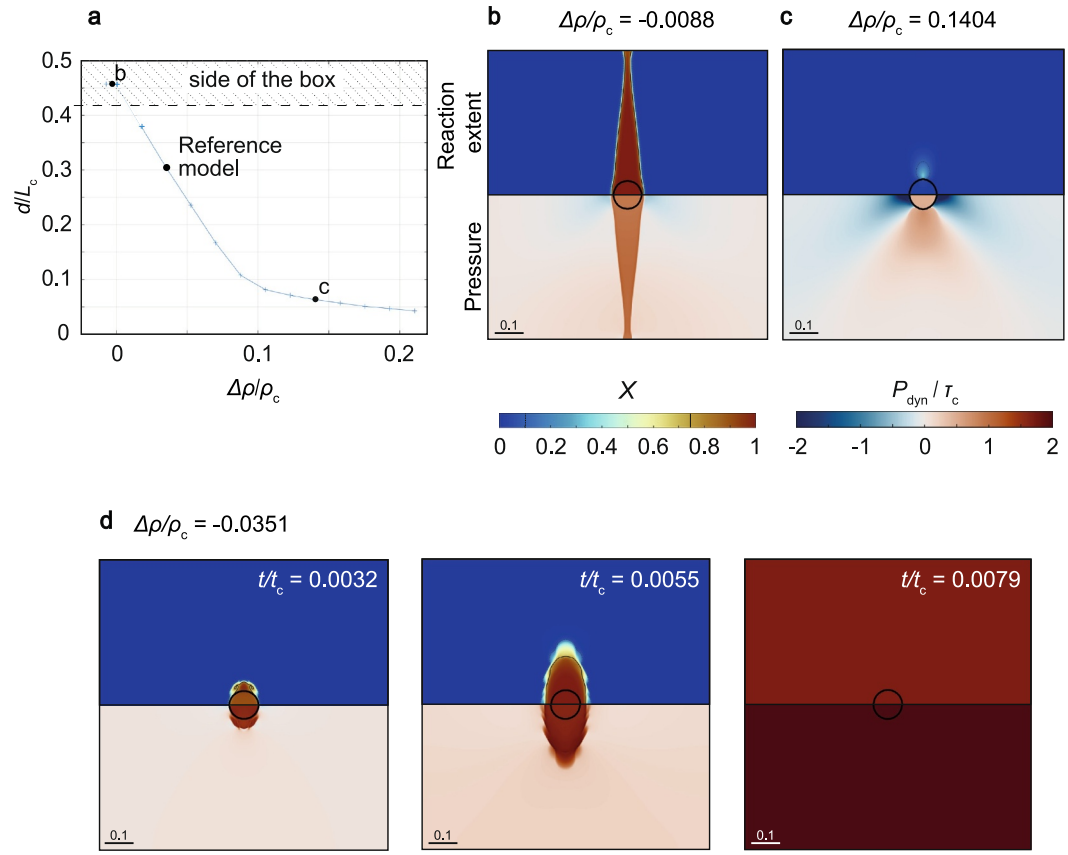


**Figure 6.** Effect of density variations caused by the transformation ($\Delta\rho$) on eclogite propagation. (a) Evolution of the length of the eclogite finger as a function of $\Delta\rho$. (b,c) Reaction extent (top) and dynamic pressure field (bottom) after $t/t_c = 0.0158$ for $\Delta\rho/\rho_c = -0.0088$ and $\Delta\rho/\rho_c = 0.1404$, respectively. (d) Same representation for important negative density change $(\Delta\rho/\rho_c = -0.0351)$ with time. The model box is entirely transformed in the last panel.

Results of these simulations show that the length of the eclogite finger increases with increasing values of the stress exponent $n$ (Figures 7c–7e).

### 3.3. Effect of the Shape of the Inclusion

To characterize the effects of the shape of the inclusion on the eclogite propagation, we carried out a parametric study on the size, aspect ratio and orientation of the inclusion. Different values were tested for (a) the radius of the inclusion (for a circular inclusion considering $b = a$, Figures 8a–8c), (b) the aspect ratio of the elliptical inclusion $a/b$ (Figures 8d–8f), and (c) the angle $\lambda$ between the major axis of the ellipse and the principal shortening direction (cf. Figures 2a and 9). The ranges of parameter values tested are provided in Table S2 in Supporting Information S1.

In models with a circular inclusion, a non-linear relationship between the length of the eclogite finger and the size of the inclusion is observed (Figure 8c). In models with an elliptical inclusion that has been chosen with orientation of its major axis at 20° from the principal shortening direction, an increase of $a/b$ leads to an increase of the eclogite finger length up to a maximum value of $a/b$ above which the length of the finger decreases (Figures 8d–8f). This is due to the finger exceeding the height of the model box and highlights the low meaning of $d/L_c$ in such a case. When the inclusion is highly elongated (with a high $a/b$ ratio), the distance between the edge of the inclusion where fingers form and the edge of the box is small. Less time is therefore necessary for the finger to reach the height of the box (Figures 8e and 8f). Several values of $b/L_c$ were tested, and reveals a similar trend in the $d/L$ curves as a function of $a/b$ for models with different $b/L_c$.

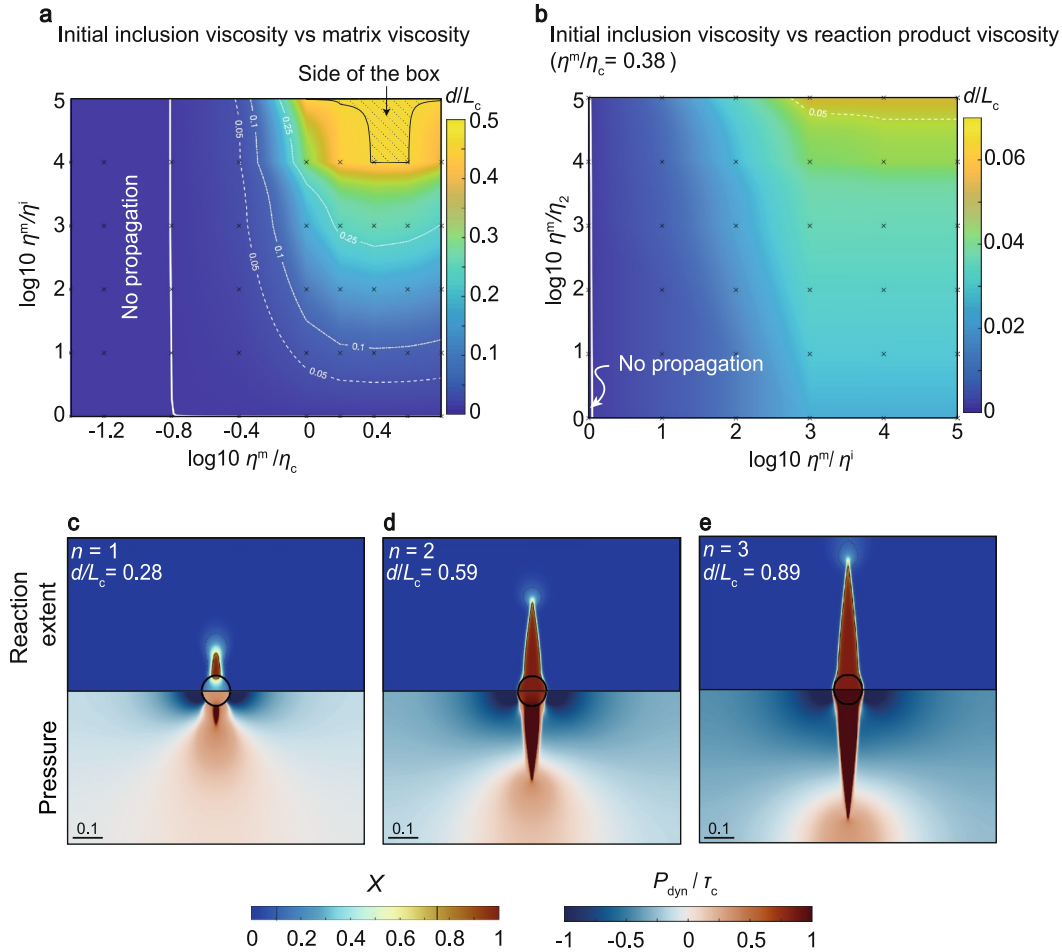


**Figure 7.** Effect of viscosity contrasts between matrix, inclusion and reaction product. (a) Length of the eclogite finger (after $t/t_c = 0.016$) for different initial viscosity contrasts between matrix and inclusion $(\eta^m/\eta^i)$ as a function of matrix viscosity $\eta^m$. The viscosity of the transformation product $\eta_2$ is equal to $\eta^i$. (b) Length of the eclogite finger (after $t/t_c = 0.016$) for different $\eta^m/\eta^i$ as a function of $\eta^m/\eta_2$. Viscosities are linear (i.e., $n = 1$) in panels (a) and (b). (c–e) Effect of non-linear viscosities ($n>1$) on the transformation propagation after $t/t_c = 0.016$. At the initial stage, $\eta^m/\eta_c = 3.8$ and $\eta^m/\eta^i = 100$ with $\eta_2 = \eta^i$.

Eventually, our results show that the orientation of the elliptical inclusion also plays a role on the eclogite propagation (Figure 9). An optimum configuration exists for finger propagation when the angle $\lambda$ between the major axis of the ellipse and the shortening direction is close to 25°–30°° (Figure 9a). For higher values of $\lambda$, finger length decreases progressively with increasing $\lambda$ until reaching a local minimum for $\lambda = 90°$. When $\lambda$ is zero, no finger is observed. A similar trend is observed for different values of $b/L_c$. The interpretation of this observation does not appear straightforward. We therefore performed simple simulations to better constrain the effect of the orientation of the weak inclusion on the pressure field (itself controlling the transformation propagation). In that prospect, simulations were performed by switching-off transformation, plasticity, elasticity and considering linear viscosities (similar to the models of Moulas et al., 2014), with $\eta^m/\eta^i = 10$ and $a/b = 5$. Results of these simulations show that the geometry of the overpressure halos (width and area) in the vicinity of the inclusion depends on its orientation (Figure 10a and Figure S2b in Supporting Information S1). From these models, we therefore extracted two parameters that characterize the overpressure halos: its area $A_{Pdyn}$, and its width $W$ defined as the distance in the shortening direction along which the edges of the ellipse are overpressured (Figure S2b in Supporting Information S1). The overpressure halos are defined as the areas where the pressure is greater than the dimensionless pressure of the transformation that equals to 3.2. By plotting $A_{Pdyn}/L_c^2$ and $W/L_c$ as a function of $\lambda$ we observe that the optimum configuration for the propagation $\lambda \sim 25°–30°$(Figure 9) corresponds to a maximum of the value of $W$. This maximum width coincides with a maximum rate of propagation

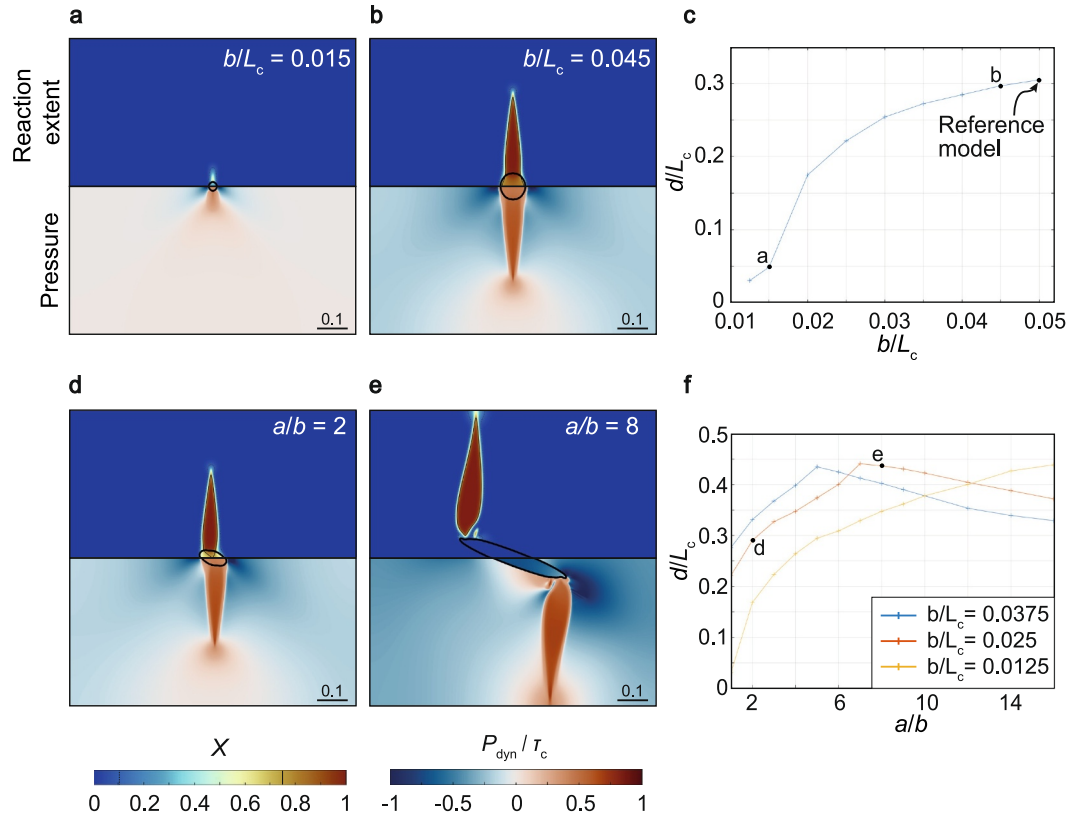


**Figure 8.** Effect of inclusion size and aspect ratio on eclogite propagation. (a, b) Transformation progress for two different sizes of a circular inclusion (at $t/t_c = 0.016$). (c) Length of the eclogite finger as a function of the inclusion radius. (d–e) Transformation progress for different aspect ratios of the elliptical inclusion $a/b$ (here, at $t/t_c = 0.016$ for $b = 0.05$ m). (f) Length of the eclogite finger as a function of $a/b$ for different values of $b$.

(blue curve Figure 10b). In detail, the propagation rate is not constant, but decreases after reaching a maximum to trend toward the rate of propagation of the simulation with $\lambda = 90°$ inclusion.

## 4. Discussion

### 4.1. Finger-Shaped Propagation of Eclogitization

#### 4.1.1. Initiation of the Transformation

This study shows that several parameters are crucial for the initiation of the transformation: (a) the viscosity of the matrix ($\eta^m$) (b) the initial viscosity contrasts between the matrix and the inclusions $\left(\eta^m/\eta^i\right)$ and (c) the difference in pressure between the pressure of the transformation and the initial background pressure ($\Delta P$).

At the studied conditions, eclogite transformation in the presence of a weak inclusion ($\eta^m/\eta^i > 1$) only initiates when $\eta^m$ is higher than $4 \times 10^{21}$ Pa.s (i.e., $10^{-0.8} \times \eta_c$, see Figure 7) and $\Delta P$ is lower than 0.6 GPa (i.e., $1.2 \times \tau_c$, see Figure 5). For lower $\eta^m$ values or greater $\Delta P$, it is not possible to generate the local overpressures required to reach the transformation pressure. In our models, overpressure is a prerequisite for the initiation of finger-like eclogite transformation. The development of this geometry is not governed by the difference between the background pressure and the pressure of transformation (i.e., $\Delta P$), since fingers can form even when $\Delta P = 0$, but rather by the pressure contrast between the surrounding matrix and the overpressure halos. The required value of $\eta^m$ (that corresponds to a $\tau_{II}$ of $\sim 80$ MPa) lies in the range of acknowledged values for the natural case study of Holsnøy considering the viscosity of dry anorthite at $\dot{\varepsilon}_{BG} = 10^{-14}$ s$^{-1}$ and $T = 700$°C (Labrousse et al., 2010; Rybacki & Dresen, 2000). It has already been proposed for the natural case study of Holsnøy, that eclogite fingers form in a context where the initial background pressure is lower than the pressure required for eclogitization to occur (Putnis et al., 2021). Based on chemical calculations, the authors show that this is possible considering a

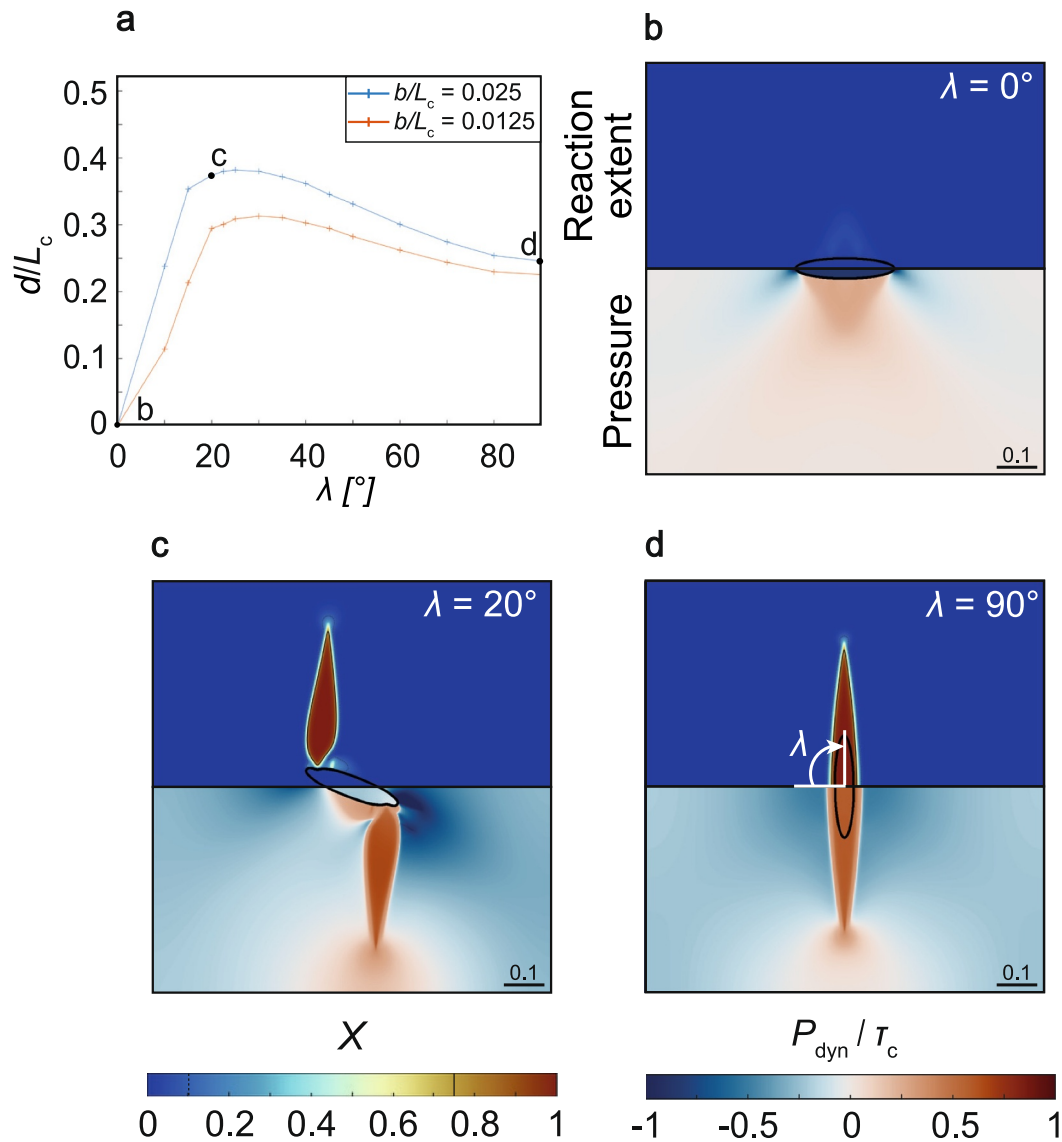


**Figure 9.** Impact of the orientation of the ellipse on eclogite propagation. (a) Length of the eclogite finger as a function of $\lambda$ for different inclusion sizes.(b–d) Transformation progress for different values of $\lambda$ (angle between the major axis of the ellipse and the principal shortening direction), considering $a/b = 5$ and $b/L_c = 0.025$ (at $t/t_c = 0.016$).

pressure variation on the order of 0.16–0.5 GPa. Our results which show that the transformation occurs for $\Delta P$ of less than 0.6 GPa are therefore in agreement with the results of this study. In addition, the values of $\Delta P$ required to initiate the transformation lies in the range of acknowledged values for the natural case study of Holsnøy considering the difference in pressure between pseudotachylyte formation in the amphibolite facies and eclogitization (difference between Stage 2 and Stage 1 in Bhowany et al. (2017)). Noteworthy, the same pattern could probably be produced with a media above reaction pressure and limited reaction kinetics, and tectonic overpressure promoting reaction via control on the kinetics activation energy. Such a model would require better knowledge of these activation energy and volume values as well as what 'pressure' actually drives reaction kinetics (Wheeler, 2014). Control of stress state orientation on eclogite reaction kinetics in Holsnøy has been addressed based on field evidence (Baïsset et al., 2025).

In our models, eclogite fingers form in response to local pressure increase, which can be generated by strain rates comparable to average geological values (Fagereng & Biggs, 2019). Eclogitization in this case is not associated with the formation of highly deformed or sheared zones, aligning with observations of a static pattern of

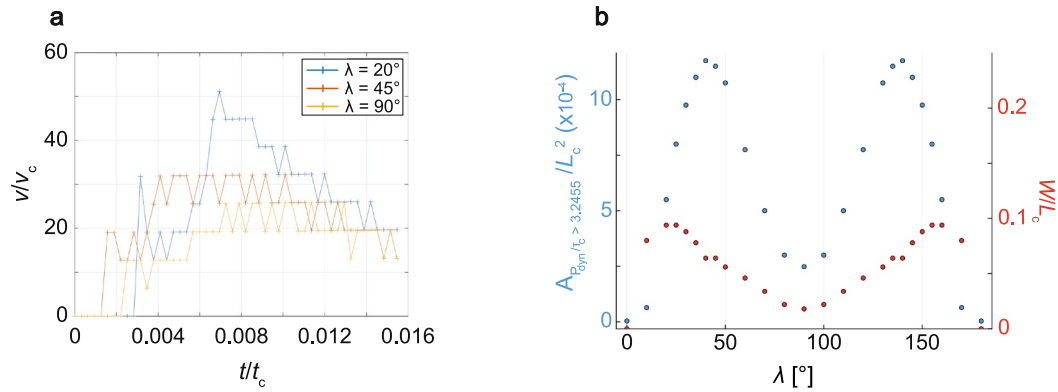


**Figure 10.** Size of the overpressure halos and propagation rate depending on ellipse orientation. (a) Evolution of the propagation rate over time for different $\lambda$ values. This graph represents the results of the reference model (i.e., a visco-elasto-viscoplastic model in which metamorphic transformation have been implemented. The rate of the propagation of the finger ($V$) is normalized to the strain rate through: $V/V_c = V/\left(L_c \times \dot{\varepsilon}_{BG}\right)$ (b) Area $\left(A_{Pdyn}/L_c^2\right)$ and width $(W/L_c)$ of the overpressure halos (i.e., areas where $P_{dyn}/\tau_c > 3.2$) as a function of the orientation of the ellipse $\lambda$ (see Figure S2 in Supporting Information S1 for calculation details). This graph represents the results of a simplified model in comparison to the reference model (see text for details). To help comparing this model with the results of Moulas et al. (2014), simulations were performed with $\eta^m/\eta^i = 10$ and $a/b = 5$.

eclogitization along fingers in Holsnøy (Austrheim, 1987; Baïsset et al., 2023, 2025; Putnis et al., 2021; Zertani et al., 2022).

### 4.1.2. Propagation of the Transformation During Bulk Shear Deformation

While $\eta^m$ and $\Delta P$ drive the initiation of the transformation, additional parameters influence the propagation of the transformation. These parameters are: (a) the density variations induced by the transformation $\Delta\rho$, (b) the viscosity ratio between the matrix and the inclusion $\eta^m/\eta^i$, (c) the viscosity variation induced by the transformation $\left(\eta_2\right)$ and (d) the shape and size of the inclusion.

#### *4.1.2.1. Direction of Propagation*

In each simulation, the direction of transformation propagation is systematically normal to the principal shortening direction (Figure S1 in Supporting Information S1). While the presence of a structural anisotropy (granulites in Holsnøy are strongly foliated) has not been implemented in our models, the production of fingers systematically propagating normal to the principal shortening direction echoes recent statistical analysis of eclogite patterns in Holsnøy (Baïsset et al., 2025). Field observations indeed indicate that fingers preferentially propagate along the granulite layering where it is oriented close to normal to the principal shortening direction. Our results show that eclogite propagation spontaneously propagate at 90° from the principal shortening direction following the anisotropy of the stress field created by the presence of mechanical heterogeneities (here the inclusion). The observation of Baïsset et al. (2025) that eclogite fingers are less prone to growth when the layering is oriented at low angle from the principal shortening direction therefore suggests that this structural anisotropy is also a major controlling factor of the transformation. This raises new questions about the nature of the anisotropy involved (e.g., a mechanical anisotropy, chemical anisotropy, anisotropy of permeability). A few studies have already started to look at such anisotropy (e.g., Baïsset et al., 2025; Putnis et al., 2021), but models accounting for anisotropy should reproduce the propagation of eclogitization under stress in the light of natural observations.

As models presented in this study are 2D, we may wonder how our results apply in 3D. Field observations actually suggest that fingers in 3D correspond to planes rather than "fingers" strictly speaking: (a) These static eclogite structures always appear as fingers in the field (hence their name) but never present tubular shapes that could indicate a real finger structure. This means that the pattern observed probably corresponds to a cross-section through a planar structure. (b) Fingers stem from eclogite shear zones which constitute planes in 3D. It seems therefore more likely that fingers also constitute 3D planes. (c) Fingers propagate normal to the principal shortening direction that is, in a plane in 3D (Baïsset et al., 2025). Hence, it seems like the finger-shaped structures

we managed to reproduce in 2D correspond to planes or flattened ellipsoïds propagating both directions normal to shortening rather than actual 3D "fingers."

#### 4.1.2.2. The Geometry of the Inclusion

An optimum configuration for propagation is observed when the elliptical inclusion is oriented at $\lambda = 25$–$30°$ from the shortening direction (Figure 9a). So, this orientation corresponds to the maximum of propagation rate (Figure 10a). In this configuration, the width of the overpressure halos also reaches a maximum (Figure 10b). This observation suggests that the propagation rate is controlled by the width of the overpressure halo rather than its area (which is not maximal when $\lambda = 25$–$30°$ (Figure 10b)). Higher propagation rates are indeed observed in the case of larger inclusions, which generate wider overpressure halos than smaller ones (Figure 8). In addition, when examining the propagation rates throughout the simulation, those associated with ellipses oriented at an angle different from 90° tend to converge toward the propagation rate with an inclusion oriented at $\lambda = 90°$ (Figure 10a). This is due to the viscosity of the matrix becoming as low as the viscosity of the inclusion after it transforms. The mechanical heterogeneity initially formed by the elliptical inclusion progressively loses its initial shape, and evolves toward a wider zone, formed by the inclusion and the transformed parts of the matrix which are oriented normal to the principal shortening direction (Figure 9c). The mechanical heterogeneity thus more closely resembles an ellipse oriented at 90° from the shortening direction. This explains why the propagation rate trends toward that of an inclusion oriented at $\lambda = 90°$.

#### 4.1.2.3. The Competing Roles of Density and Viscosity Variations

In the case of a densification transformation ($\Delta\rho > 0$), mass balance implies that a density increase leads to a volume decrease. This volume decrease generates a decrease in pressure in the whole model (Yamato et al., 2022). The pressure of the transformation is therefore rarely reached in this case and the propagation of the transformation is consequently inhibited. Densification can therefore be considered as a limiting factor for the eclogite propagation. It does not totally hinder the transformation but it limits the rate at which the transformation front progresses. In contrast, in the case of negative $\Delta\rho$ values, the propagation is very fast. These results could explain why meter-scale finger-shaped eclogite structures are observed in Holsnoy, while amphibolitization, which has a net negative $\Delta\rho$, instead spreads over large areas (Centrella et al., 2015).

The rate of transformation is also controlled by the viscosity ratio between the matrix and the inclusion. As already shown by Schmid and Podladchikov (2003), and Moulas et al. (2014), the higher this ratio, the higher the local overpressures at the tip of the inclusion and, in our case, the higher the propagation rate. The effect of $\eta^m/\eta^i$ on the propagation rate therefore compares with the effect of $\Delta\rho$ as it controls the amplitude of local pressure variations at the tip of the finger. Viscosity variations associated with the transformation not only influence the propagation velocity but are also essential for the initiation of the propagation. Indeed, overpressured zones propagate because the transformed regions weaken and approach the viscosity of the inclusion. The weak area of the model (which is initially composed by the inclusion only) therefore enlarges with time. Regardless of the value of $\Delta P$ or of the initial viscosity contrast between the inclusion and the matrix, propagation only occurs when a significant contrast exists between the matrix and the transformation product (Figure S6 in Supporting Information S1).

Eventually, our results show that the propagation rate of the fingers reaches a steady-state regime after a rapid initial increase (Figure S4 in Supporting Information S1). However, this observation does not apply in certain extreme cases, such as when a strong viscosity contrast is imposed between the matrix and the inclusion, or when a high stress exponent is used in the strain rate-dependent equations of the viscosity (Equation 15; Figure S4 in Supporting Information S1). This steady state highlights the coupled nature of the processes in these models, and particularly the roles of viscosity ratios and density, which respectively promote and inhibit propagation for larger values. Moreover, the average propagation rates are one to two orders of magnitude higher than the background strain rate. This suggests, considering that fluids are not a limiting factor, that propagation rates that compare to natural strain rates are necessary for eclogite fingers to form and be preserved as isolated structures in Holsnøy. In contrast, in the case of very high propagation rates fingers would unlikely be observed in the field, as the granulite would have been entirely transformed, similarly to the results of models with a negative density change.

In our reference model, we set the densification value to 100 $kg.m^{-3}$. Although this represents a lower bound for eclogitization, it is likely that the actual densification is higher (Deer et al., 2013). Our parametric study shows

that the density contrast slows down the transformation (Figure 6), but does not prevent the development of finger-like structures (see Figure S7 in Supporting Information S1). Since the timing of this process is uncertain due to unknown reaction kinetics, we chose a densification of 100 kg.m$^{-3}$, which allows us to investigate the growth of finger-like structures while keeping the computational cost manageable.

#### *4.1.2.4. Implications for Our Understanding of Lower Crustal Structures and Stress State*

In theory, the anisotropy of eclogite propagation could potentially be detected by geophysical methods as the difference in texture and density between eclogite and granulite is significant. This has been addressed at different scales within the Holsnøy massif by previous studies (Labrousse et al., 2010; Zertani, John, et al., 2019) They point at the smoothing effect of P and S waves, which for kilometer wavelengths would average the properties of any meter to decameter-scale structure. Concerning the anisotropy of the stress state, a geometric relationship can be observed between shear zones and fingers in Holsnøy, although the latter are not all oriented in the same direction (Baïsset et al., 2025). This raises the question of the variability of the local stress field. Indeed, fingers form series of parallel structures, but they are oriented in different directions depending on the location of the outcrops along the island. Therefore we cannot expect a pronounced regional anisotropy induced by these eclogite fingers at the scale of the whole island. Larger scale shear zones actually bear the most significant fabric (Zertani, John, et al., 2019).

### 4.2. Comparaison With Previous Studies

Our model involves a 'simplified' metamorphic transformation that initiates at a given pressure for a given temperature. In nature however, eclogitization is instead a complex process that involves a series of successive reactions with different kinetics and different mechanical consequences over a range of increasing pressure conditions (e.g., Austrheim & Griffin, 1985). It has even been proposed that the transient mineralogical assemblage of the rock undergoing transformation could be weaker than both the protolith and the final mineralogical assemblage (Bras et al., 2021). Such a late re-hardening of the material would not drastically change our results because local pressure variations are only required to initiate the transformation at the tip of the inclusion/finger. Such pressure variation would still occur in the presence of a weak material (even though transient) inside a stronger matrix, whatever the final viscosity of the reaction product.

The model we propose here neglects the effect of fluid migration in the system. When neglecting porosity and/or permeability anisotropy, fluids would flow from high-pressure regions to low-pressure regions, that is, away from the overpressure halo, thereby helping the propagation of the reaction front. As the finger tips correspond to the areas with the steepest pressure gradients, outward fluid flow may actually contribute to reinforcing the finger-shaped geometry. Very few numerical studies focused on the mechanism of formation of finger-shaped reactive structures in the presence of fluids. Analog numerical models of eclogitization under shear conditions (Jamtveit et al., 2000) showed that transformation-induced volume reduction is able to generate significant local stresses for the yield stress of the rock to be reached. In these models, fluids penetrate into the newly formed fractures, and allow eclogitization of the material. Reaction-induced volume reduction then promotes fracturing in a self-sustained process. Cylindrical eclogitization fronts form in all their models, except when an anisotropic stress field is imposed. In that case, finger-shaped eclogite fronts develop. Recent numerical studies also tackle the issue of the propagation of eclogite transformation (Bras et al., 2023; Schmalholz et al., 2024). These studies present the results of hydro-mechanical-chemical models where densification is associated with an increase of the permeability of the rock. Fluid pressure gradients in the newly formed porosity then enhances fluid flow and therefore the propagation of the transformation.

In our simulations, densification hinders the propagation of the finger because it decreases the pressure throughout the model. This contrasts with the model of Jamtveit et al. (2000), where volume reduction increases local stresses and thus promotes the propagation of eclogite fingers. Our results also differ from those of Bras et al. (2023) and Schmalholz et al. (2024), who identify the density change as the driving mechanism for eclogite propagation. It is therefore conceivable that densification associated with eclogitization could simultaneously facilitate fluid migration while hindering the propagation of the transformation itself by reducing the pressure required for transformation (fluid pressure or solid pressure).

Our study shows that transformation-induced softening (decrease of the viscosity of the transformation product compared to the initial viscosity of the matrix) is necessary to propagate overpressures in the matrix, and

consequently initiate the propagation of the eclogite transformation. Interesting comparison can be made with models where the transformation is associated with a hardening of the transformed areas compared to the initial matrix (e.g., Schmalholz et al., 2023). In the models of Schmalholz et al. (2023), the transformation studied (serpentinite dehydration) involves a positive density change as it is the case for eclogitization, but is accompanied by an increase in viscosity of the transformation product. In this configuration, transformation propagates in the direction of shortening in opposition to the results of the present study. This difference is explained by the role of viscosity variations in controlling the geometry of the overpressure halo. Indeed, previous numerical studies (Moulas et al., 2014; Schmid & Podladchikov, 2003) already showed that when the viscosity of the transformation product is higher than that of the matrix, the overpressure halos are elongated in the shortening direction; while they are elongated normal to the shortening direction when the transformation product is weaker than the matrix. A significant difference between the present study and previous ones is the pressure controlling the reaction: solid pressure (our study) versus fluid pressure (Schmalholz et al., 2023). Since both types of models lead to transformation propagation, it seems that both fluid pressure and solid pressure can trigger and control transformation propagation. It would therefore be valuable to develop hydro-chemo-mechanical models that account for metamorphic transformations dependent on both fluid and solid pressure to properly determine and quantify the actual contribution of both mechanisms.

## 5. Conclusion

This study proposes a series of 2D thermo-mechanical numerical simulations that simulate the initiation and propagation of eclogitization in granulite-facies rocks from the lower continental crust. We model the deformation of a weak inclusion embedded in a stronger matrix, at conditions were both inclusion and matrix can transform when the required pressure for the transformation is reached. An intensive parametric study of the main physical parameters that control the mechanical behavior of the rocks has been performed. We show that the pressure variations and the viscosity of the protolith play a significant role in the initiation and propragation of eclogitization. Meanwhile, the density and viscosity variations caused by the transformation, as well as the morphology of the inclusion only control the rate of propagation of the transformation.

## Conflict of Interest

The authors declare no conflicts of interest relevant to this study.

## Data Availability Statement

The data of this study have been generated by using the code MDoodz7.0. This code is freely accessible and all the information needed to install the code and use it is available through Zenodo (Cochet et al., 2025). The Matlab file used to read the Output files is also given. In addition, Output data are provided for the reference model (Cochet et al., 2025).

**Acknowledgments**
This work was carried out as part of the METROLOGY project supported by the ANR (ANR-23-CE49-0008). It is also the fruit of a collaborative effort highly facilitated by the Heraeus Foundation endowed visiting professorship to P.Y. at the Institute of Geosciences of Goethe University Frankfurt (Frankfurt am Main, Germany). We thank S. Schorn, an anonymous reviewer and the associate editor, for their very constructive suggestions that truly helped us to improve the manuscript.

## References

Austrheim, H. (1987). Eclogitization of lower crustal granulites by fluid migration through shear zones. *Earth and Planetary Science Letters*, *81*(2–3), 221–232. https://doi.org/10.1016/0012-821x(87)90158-0

Austrheim, H., & Boundy, T. (1994). Pseudotachylytes generated during seismic faulting and eclogitization of the deep crust. *Science*, *265*(5168), 82–83. https://doi.org/10.1126/science.265.5168.82

Austrheim, H., & Griffin, W. L. (1985). Shear deformation and eclogite formation within granulite-facies anorthosites of the Bergen arcs, western Norway. *Chemical Geology*, *50*(1–3), 267–281. https://doi.org/10.1016/0009-2541(85)90124-x

Baïsset, M. (2023). *Déformation et transformations du plagioclase sous contrainte: implications pour la rhéologie de la croûte continentale inférieure à haute pression* (Doctoral dissertation). Sorbonne Université.

Baïsset, M., Labrousse, L., Yamato, P., & Cochet, A. (2025). Stress-controlled reaction pattern in the layered lower crust: Field evidence. *Earth and Planetary Science Letters*, *657*, 119270. https://doi.org/10.1016/j.epsl.2025.119270

Baïsset, M., Labrousse, L., Yamato, P., & Schubnel, A. (2023). Twinning and partial melting as early weakening processes in plagioclase at high pressure: Insights from Holsnøy (Scandinavian Caledonides, Norway). *Contributions to Mineralogy and Petrology*, *178*(3), 19. https://doi.org/10.1007/s00410-023-01998-x

Bhowany, K., Hand, M., Clark, C., Kelsey, D. E., Reddy, S. M., Pearce, M. A., et al. (2017). Phase equilibria modelling constraints on P–T conditions during fluid catalysed conversion of granulite to eclogite in the Bergen Arcs, Norway. *Journal of Metamorphic Geology*, *36*(3), 315–342. https://doi.org/10.1111/jmg.12294

Bras, E., Baïsset, M., Yamato, P., & Labrousse, L. (2021). Transient weakening during the granulite to eclogite transformation within hydrous shear zones (Holsnøy, Norway). *Tectonophysics*, *819*, 229026.

Bras, E., Yamato, P., Schmalholz, S. M., Duretz, T., & Podladchikov, Y. Y. (2023). Eclogitisation of dry and impermeable granulite by fluid flow with reaction-induced porosity: Insights from hydro-chemical modelling. *Earth and Planetary Science Letters*, *617*, 118256. https://doi.org/10.1016/j.epsl.2023.118256

Brodie, K., & Rutter, E. (1987). The role of transiently fine-grained reaction products in syntectonic metamorphism: Natural and experimental examples. *Canadian Journal of Earth Sciences*, *24*(3), 556–564. https://doi.org/10.1139/e87-054

Byerlee, J. (1978). Friction of rocks. In *Rock friction and earthquake prediction* (pp. 615–626).

Centrella, S., Austrheim, H., & Putnis, A. (2015). Coupled mass transfer through a fluid phase and volume preservation during the hydration of granulite: An example from the Bergen Arcs, Norway. *Lithos*, *236*, 245–255. https://doi.org/10.1016/j.lithos.2015.09.010

Cochet, A., Yamato, P., Baïsset, M., Duretz, T., & Labrousse, L. (2025). Files relative to mdoodz7.0 code used in cochet et al. paper entitled "what controls finger-shaped transformation patterns? a numerical approach to eclogitization " [Software]. *Zenodo*. https://doi.org/10.5281/zenodo.15426736

Deer, W. A., Howie, R. A., & Zussman, J. (2013). *An introduction to the rock-forming minerals*. Mineralogical Society of Great Britain and Ireland.

Duretz, T., de Borst, R., & Yamato, P. (2021). Modeling lithospheric deformation using a compressible visco-elasto-viscoplastic rheology and the effective viscosity approach. *Geochemistry, Geophysics, Geosystems*, *22*(8), e2021GC009675. https://doi.org/10.1029/2021gc009675

Duretz, T., de Borst, R., Yamato, P., & Le Pourhiet, L. (2020). Toward robust and predictive geodynamic modeling: The way forward in frictional plasticity. *Geophysical Research Letters*, *47*(5), e2019GL086027. https://doi.org/10.1029/2019gl086027

Duretz, T., Räss, L., Podladchikov, Y., & Schmalholz, S. (2019). Resolving thermomechanical coupling in two and three dimensions: Spontaneous strain localization owing to shear heating. *Geophysical Journal International*, *216*(1), 365–379. https://doi.org/10.1093/gji/ggy434

England, P. C., & Thompson, A. B. (1984). Pressure—Temperature—time paths of regional metamorphism I. Heat transfer during the evolution of regions of thickened continental crust. *Journal of Petrology*, *25*(4), 894–928. https://doi.org/10.1093/petrology/25.4.894

Fagereng, Å., & Biggs, J. (2019). New perspectives on 'geological strain rates' calculated from both naturally deformed and actively deforming rocks. *Journal of Structural Geology*, *125*, 100–110. https://doi.org/10.1016/j.jsg.2018.10.004

Gerya, T. (2019). *Introduction to numerical geodynamic modelling*. Cambridge University Press.

Hacker, B. R., Peacock, S. M., Abers, G. A., & Holloway, S. D. (2003). Subduction factory 2. Are intermediate-depth earthquakes in subducting slabs linked to metamorphic dehydration reactions? *Journal of Geophysical Research*, *108*(B1). https://doi.org/10.1029/2001jb001129

Hetényi, G., Chanard, K., Baumgartner, L. P., & Herman, F. (2021). Metamorphic transformation rate over large spatial and temporal scales constrained by geophysical data and coupled modelling. *Journal of Metamorphic Geology*, *39*(9), 1131–1143. https://doi.org/10.1111/jmg.12604

Holyoke III, C. W., & Tullis, J. (2006). Mechanisms of weak phase interconnection and the effects of phase strength contrast on fabric development. *Journal of Structural Geology*, *28*(4), 621–640. https://doi.org/10.1016/j.jsg.2006.01.008

Huet, B., Yamato, P., & Grasemann, B. (2014). The minimized power geometric model: An analytical mixing model for calculating polyphase rock viscosities consistent with experimental data. *Journal of Geophysical Research: Solid Earth*, *119*(4), 3897–3924. https://doi.org/10.1002/2013jb010453

Jackson, J., Austrheim, H., McKenzie, D., & Priestley, K. (2004). Metastability, mechanical strength, and the support of mountain belts. *Geology*, *32*(7), 625–628. https://doi.org/10.1130/g20397.1

Jamtveit, B., Austrheim, H., & Malthe-Sørenssen, A. (2000). Accelerated hydration of the earth's deep crust induced by stress perturbations. *Nature*, *408*(6808), 75–78. https://doi.org/10.1038/35040537

Jung, H., & Green, H. W. (2004). Experimental faulting of serpentinite during dehydration: Implications for earthquakes, seismic low-velocity zones, and anomalous hypocenter distributions in subduction zones. *International Geology Review*, *46*(12), 1089–1102. https://doi.org/10.2747/0020-6814.46.12.1089

Kirby, S. H., Stein, S., Okal, E. A., & Rubie, D. C. (1996). Metastable mantle phase transformations and deep earthquakes in subducting oceanic lithosphere. *Reviews of Geophysics*, *34*(2), 261–306. https://doi.org/10.1029/96rg01050

Labrousse, L., Hetényi, G., Raimbourg, H., Jolivet, L., & Andersen, T. B. (2010). Initiation of crustal-scale thrusts triggered by metamorphic reactions at depth: Insights from a comparison between the Himalayas and Scandinavian Caledonides. *Tectonics*, *29*(5). https://doi.org/10.1029/2009tc002602

Lund, M. G., & Austrheim, H. (2003). High-pressure metamorphism and deep-crustal seismicity: Evidence from contemporaneous formation of pseudotachylytes and eclogite facies coronas. *Tectonophysics*, *372*(1–2), 59–83. https://doi.org/10.1016/s0040-1951(03)00232-4

Lund, M. G., Austrheim, H., & Erambert, M. (2004). Earthquakes in the deep continental crust-insights from studies on exhumed high-pressure rocks. *Geophysical Journal International*, *158*(2), 569–576. https://doi.org/10.1111/j.1365-246x.2004.02368.x

Malvoisin, B., Austrheim, H., Hetényi, G., Reynes, J., Hermann, J., Baumgartner, L. P., & Podladchikov, Y. Y. (2020). Sustainable densification of the deep crust. *Geology*, *48*(7), 673–677. https://doi.org/10.1130/g47201.1

Moulas, E., Burg, J.-P., & Podladchikov, Y. (2014). Stress field associated with elliptical inclusions in a deforming matrix: Mathematical model and implications for tectonic overpressure in the lithosphere. *Tectonophysics*, *631*, 37–49. https://doi.org/10.1016/j.tecto.2014.05.004

Poirier, J. (1982). On transformation plasticity. *Journal of Geophysical Research*, *87*(B8), 6791–6797. https://doi.org/10.1029/jb087ib08p06791

Putnis, A., Jamtveit, B., & Austrheim, H. (2017). Metamorphic processes and seismicity: The bergen arcs as a natural laboratory. *Journal of Petrology*, *58*(10), 1871–1898. https://doi.org/10.1093/petrology/egx076

Putnis, A., Moore, J., Prent, A. M., Beinlich, A., & Austrheim, H. (2021). Preservation of granulite in a partially eclogitized terrane: Metastable phenomena or local pressure variations? *Lithos*, *400*, 106413. https://doi.org/10.1016/j.lithos.2021.106413

Rybacki, E., & Dresen, G. (2000). Dislocation and diffusion creep of synthetic anorthite aggregates. *Journal of Geophysical Research*, *105*(B11), 26017–26036. https://doi.org/10.1029/2000jb900223

Rybacki, E., & Dresen, G. (2004). Deformation mechanism maps for feldspar rocks. *Tectonophysics*, *382*(3–4), 173–187. https://doi.org/10.1016/j.tecto.2004.01.006

Schmalholz, S. M., & Fletcher, R. C. (2011). The exponential flow law applied to necking and folding of a ductile layer. *Geophysical Journal International*, *184*(1), 83–89. https://doi.org/10.1111/j.1365-246x.2010.04846.x

Schmalholz, S. M., Khakimova, L., Podladchikov, Y., Bras, E., Yamato, P., & John, T. (2024). (de) hydration front propagation into zero-permeability rock. *Geochemistry, Geophysics, Geosystems*, *25*(9), e2023GC011422. https://doi.org/10.1029/2023gc011422

Schmalholz, S. M., Moulas, E., Räss, L., & Müntener, O. (2023). Serpentinite dehydration and olivine vein formation during ductile shearing: Insights from 2D numerical modeling on porosity generation, density variations, and transient weakening. *Journal of Geophysical Research: Solid Earth*, *128*(11), e2023JB026985. https://doi.org/10.1029/2023jb026985

Schmid, D. W., & Podladchikov, Y. Y. (2003). Analytical solutions for deformable elliptical inclusions in general shear. *Geophysical Journal International*, *155*(1), 269–288. https://doi.org/10.1046/j.1365-246x.2003.02042.x

Shi, F., Wang, Y., Yu, T., Zhu, L., Zhang, J., Wen, J., et al. (2018). Lower-crustal earthquakes in southern Tibet are linked to eclogitization of dry metastable granulite. *Nature Communications*, *9*(1), 3483. https://doi.org/10.1038/s41467-018-05964-1

Wheeler, J. (2014). Dramatic effects of stress on metamorphic reactions. *Geology*, *42*(8), 647–650. https://doi.org/10.1130/g35718.1

Yamato, P., Duretz, T., & Angiboust, S. (2019). Brittle/ductile deformation of eclogites: Insights from numerical models. *Geochemistry, Geophysics, Geosystems*, *20*(7), 3116–3133. https://doi.org/10.1029/2019gc008249

Yamato, P., Duretz, T., Baïsset, M., & Luisier, C. (2022). Reaction-induced volume change triggers brittle failure at eclogite facies conditions. *Earth and Planetary Science Letters*, *584*, 117520. https://doi.org/10.1016/j.epsl.2022.117520

Zertani, S., John, T., Brachmann, C., Vrijmoed, J. C., & Plümper, O. (2022). Reactive fluid flow guided by grain-scale equilibrium reactions during eclogitization of dry crustal rocks. *Contributions to Mineralogy and Petrology*, *177*(6), 61. https://doi.org/10.1007/s00410-022-01928-3

Zertani, S., John, T., Tilmann, F., Motra, H. B., Keppler, R., Andersen, T. B., & Labrousse, L. (2019). Modification of the seismic properties of subducting continental crust by eclogitization and deformation processes. *Journal of Geophysical Research: Solid Earth*, *124*(9), 9731–9754. https://doi.org/10.1029/2019jb017741

Zertani, S., Labrousse, L., John, T., Andersen, T. B., & Tilmann, F. (2019). The interplay of eclogitization and deformation during deep burial of the lower continental crust—A case study from the Bergen arcs (western Norway). *Tectonics*, *38*(3), 898–915. https://doi.org/10.1029/2018tc005297

Zhang, J., Green II, H. W., & Bozhilov, K. N. (2006). Rheology of omphacite at high temperature and pressure and significance of its lattice preferred orientations. *Earth and Planetary Science Letters*, *246*(3–4), 432–443. https://doi.org/10.1016/j.epsl.2006.04.006